

Salty neutrinos from the Sun

Results from the salt phase of the Sudbury Neutrino Observatory

S.J.M. Peeters^a

For the SNO Collaboration

University of Oxford, Particle Physics, Denys Wilkinson Building, Keble Road, Oxford, OX1 3RH, UK

Received: 1 July 2005 /

Published online: 10 February 2006 – © Società Italiana di Fisica / Springer-Verlag 2006

Abstract. The Sudbury Neutrino Observatory is a 1 ktonne heavy-water Čerenkov detector. The first phase of this experiment has shown that neutrinos from the Sun change flavour. For the second phase of the experiment, approximately 2 tonnes of salt (NaCl) was added to the heavy water to enhance the neutral-current detection as well as the neutral-current and charged-current separability. Here the results are presented from the complete salt phase at the Sudbury Neutrino Observatory. The electron energy spectrum is presented for the first time. It is consistent with an undistorted ${}^8\text{B}$ spectral shape. It is also consistent with the Large Mixing Angle (LMA) parameters obtained through a global fit including the data presented in this paper. These parameters are found to be $\Delta m^2 = (8.0_{-0.4}^{+0.6}) \times 10^{-5} \text{ eV}^2$ and $\theta = 33.9_{-2.2}^{+2.4}$ degrees. The total flux of active-flavour neutrinos from ${}^8\text{B}$ decay in the Sun is found to be $4.94_{-0.21}^{+0.21}(\text{stat})_{-0.34}^{+0.38}(\text{syst})$, whereas the integral flux of electron neutrinos for an undistorted ${}^8\text{B}$ spectrum is $1.68_{-0.06}^{+0.06}(\text{stat})_{-0.09}^{+0.08}(\text{syst})$, both in units of $10^6 \text{ cm}^{-2} \text{ s}^{-1}$. The day-night asymmetry in the observed fluxes is consistent with both absence of matter-enhancement effects in the Earth and with the small level of these effects expected for the LMA model as stated above.

PACS. 26.65.+t Solar neutrinos – 14.60.Pq Neutrino mass and mixing

1 Introduction

Ray Davis' experiment [1] indicated over 35 years ago that the observed electron neutrino flux from the Sun was lower than expected from the Standard Solar Model [2]. As it was thought that the physics of Sun was well understood, this discrepancy was deemed “the solar neutrino problem”.

In the first “D₂O” phase of the Sudbury Neutrino Observatory (SNO), the long-standing solar neutrino problem was solved. It demonstrated (see [3]) that the total active neutrino flux from the Sun, observed via neutral-current (NC) reactions, is consistent with Standard Solar Model (SSM), whereas the electron neutrino component of this flux, observed via charged-current (CC) reactions, is indeed too low. This shows that neutrinos change flavour on their way from the Sun to the Earth and thus solved the solar neutrino problem.

In the second “salt” phase of SNO, 2 tonnes of ultra-pure salt (NaCl) was dissolved into the heavy water. This enhanced the detection efficiency of the NC flux, but more importantly this increased the separability of the CC reactions and the NC reactions. The results of the first 254

days of data of this phase were published in [4]. Recently, the results of the full 391 days of data of this phase were published [5] and these results will be discussed in this article.

Finally, the third (“NCD”) phase of SNO has started recently. In this phase 40 ${}^3\text{He}$ proportional counters (neutral-current detectors or “NCDs”) have been placed inside the heavy-water volume. These absorb and detect the neutrons (produced by NC reactions) within the heavy-water volume and will allow an even better separation of NC events and CC events.

2 The Sudbury Neutrino Observatory

SNO [6] is a 1 ktonne water Čerenkov detector, located at a depth of 2092 m (6010 m of water equivalent) in the INCO Ltd. Creighton mine near Sudbury, Ontario in Canada. The detector (see fig. 1) consists of a 5.5 cm thick, 12 m diameter acrylic vessel (AV), holding the 1000 tonnes ultra-pure D₂O target, surrounded by 7 ktonnes of ultra-pure H₂O shielding. The AV is surrounded by a 17.8 m diameter geodesic sphere, holding 9456 inward-looking and 91 outward-looking 20 cm photomultiplier tubes (PMTs).

^a e-mail: s.peeters1@physics.ox.ac.uk

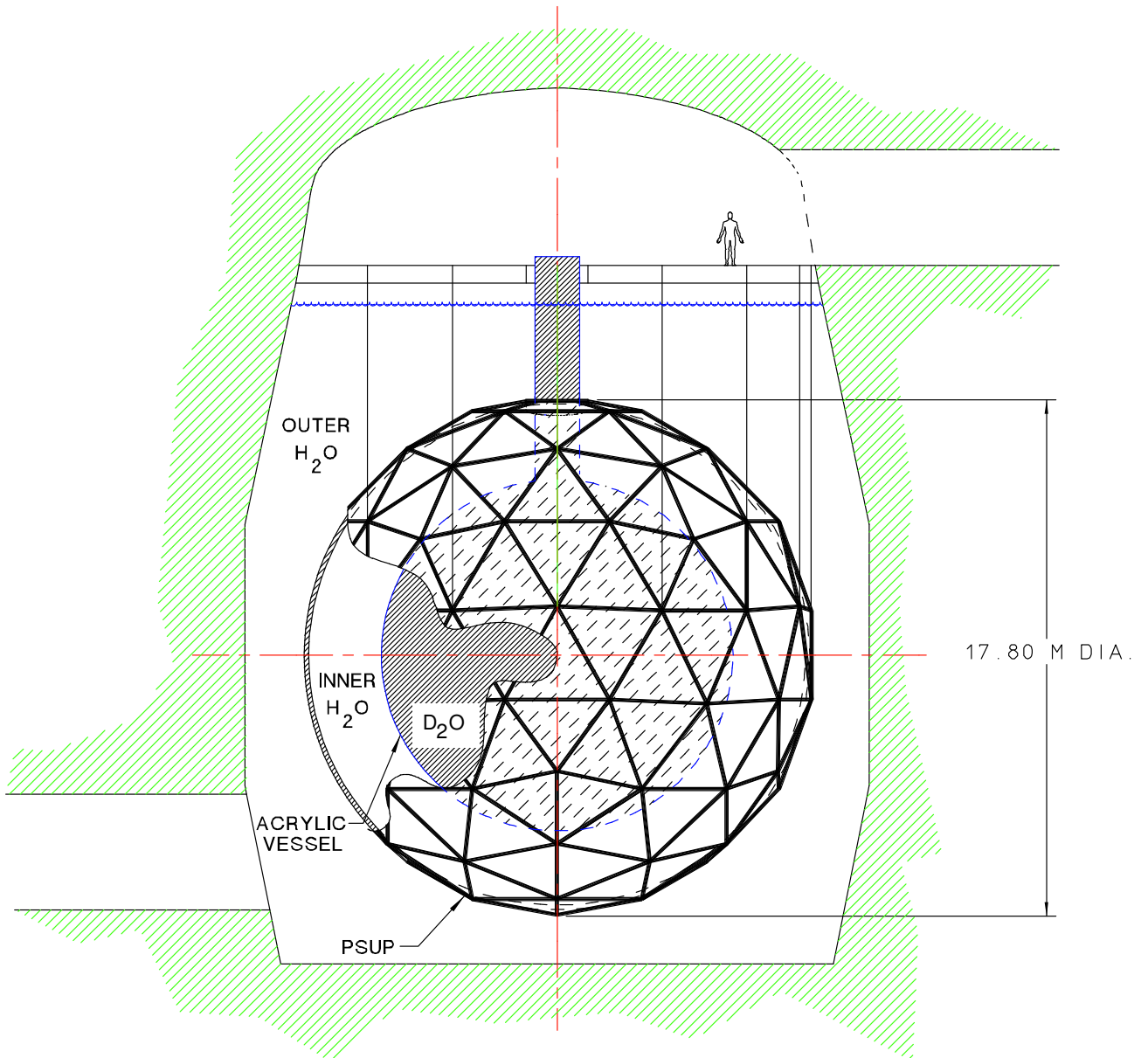


Fig. 1. The layout of the SNO detector. The PSUP holds the photomultiplier tubes.

The PMTs are surrounded by light concentrators, which increase the light collection efficiency. The effective coverage is 59%. The volume outside the geodesic support structure acts both as a cosmic-ray veto system and as a shield from naturally occurring radioactivity from the surrounding rock and the construction materials.

SNO detects neutrinos via elastic scattering (ES, $\nu_x + e^- \rightarrow \nu_x + e^-$, $x = e, \mu, \tau$), CC ($\nu_e + d \rightarrow p + p + e^-$) and NC ($\nu_x + d \rightarrow n + p + \nu_x$). The elastic scattering is sensitive to all neutrino flavours, but the electron neutrino reaction is enhanced by a factor of approximately 6.5 compared to the other flavours. The CC reaction is only sensitive to electron neutrinos. The NC reaction, however, is equally sensitive to all active neutrino flavours.

The ES and CC events are observed by the Čerenkov light generated by the electron produced in these reactions. The NC events are observed more indirectly. The neutron captures on either deuterium (first (pure D₂O) phase) or chlorine (second (salt) phase) creating an excited state which decays emitting γ 's. These γ 's primarily Compton-scatter, producing relativistic electrons, which produce observable Čerenkov light.

2.1 Neutrino detection in the salt phase

Adding ultra-pure NaCl to the heavy-water target to a concentration of $(0.196 \pm 0.002)\%$ by weight increases the detection efficiency for neutrons, and thus the sensitivity

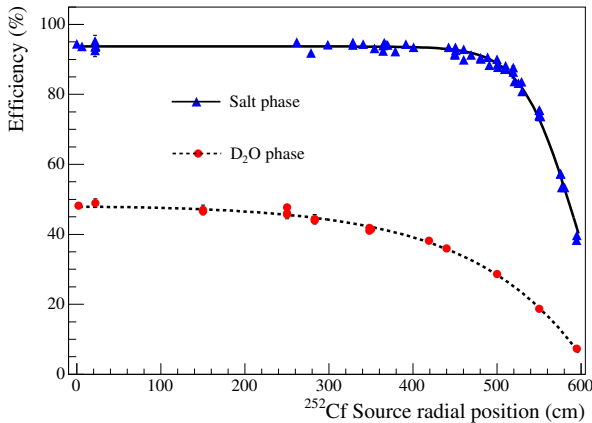


Fig. 2. Neutron capture efficiency *versus* radial position of the ^{252}Cf source for the pure D_2O and salt phase.

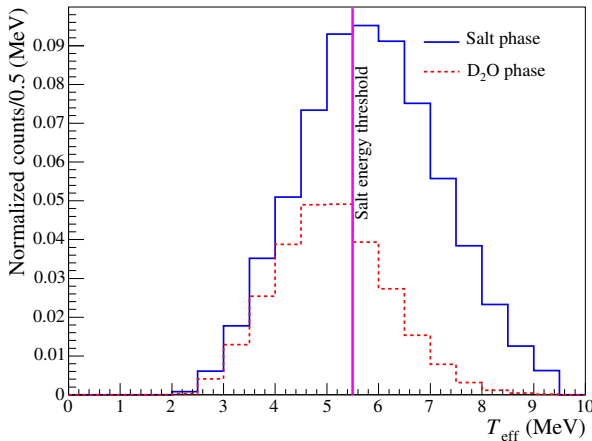


Fig. 3. Neutron energy response during the D_2O (dashed line) and salt (solid line) running periods. The vertical line represents the analysis energy threshold of $T_{\text{eff}} = 5.5$ MeV. The distributions shown here are normalised to the neutron detection efficiency in the two phases for $R < 550$ cm.

to the NC reaction is enhanced. This increase of detection efficiency comes about from two effects.

Firstly, the neutron capture cross-section of deuterium is 0.5 mbarn, whereas the neutron capture cross-section of ^{35}Cl is 44 barn. Figure 2 shows a comparison of the neutron capture efficiency for the D_2O phase and the salt phase, as measured using calibration sources in SNO. It clearly shows a large increase neutron capture efficiency in the salt phase, compared to the D_2O phase.

Secondly, when a neutron captures on deuterium, a single γ of 6.25 MeV is emitted. In the salt phase, for a neutron produced within the AV, the probability of capture on ^{35}Cl is 90%. When a neutron captures on ^{35}Cl , multiple γ 's are released with a total energy of 8.6 MeV. As shown in fig. 3, this enhances the detection probability, as more Čerenkov light is produced.

In the salt phase, neutron capture is observed by the Čerenkov light produced by relativistic electrons produced

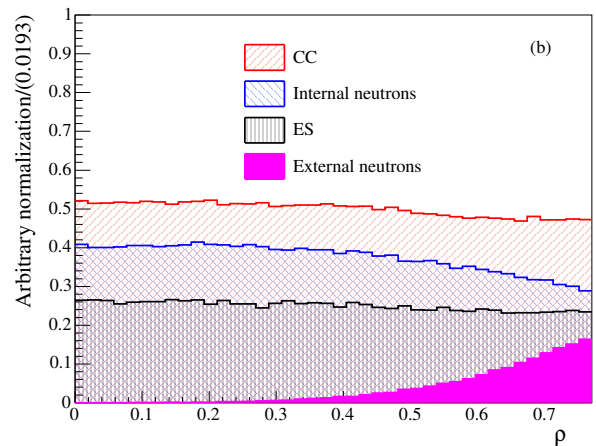
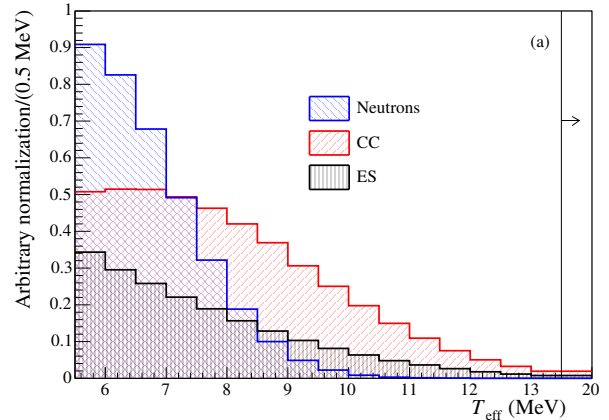


Fig. 4. T_{eff} (a) and ρ (b) distributions for NC, CC, ES, and external neutron events. Where internal and external distributions are identical the distribution is simply labeled neutrons. Note that the distribution normalizations are arbitrary and chosen to allow the shape differences to be seen clearly. The CC energy spectrum shape corresponds to an undistorted ^8B model.

by multiple γ 's produced from the neutron capture on ^{35}Cl , instead of the single γ produced with neutron capture on D_2O . The isotropy of the hit distribution on the PMT array from the multiple γ -rays emitted from capture on ^{35}Cl is significantly different from that produced by a single relativistic electron (see fig. 5(a)). This extra information allows statistical separation of electrons created by the CC interactions and neutrons from NC interactions *without* any assumptions on the underlying neutrino energy distributions.

3 Data analysis

3.1 Signal extraction

Figures 4 and 5 show the four observables used to statistically separate the signals due to the three types of neutrino interaction. The variables used are derived from the

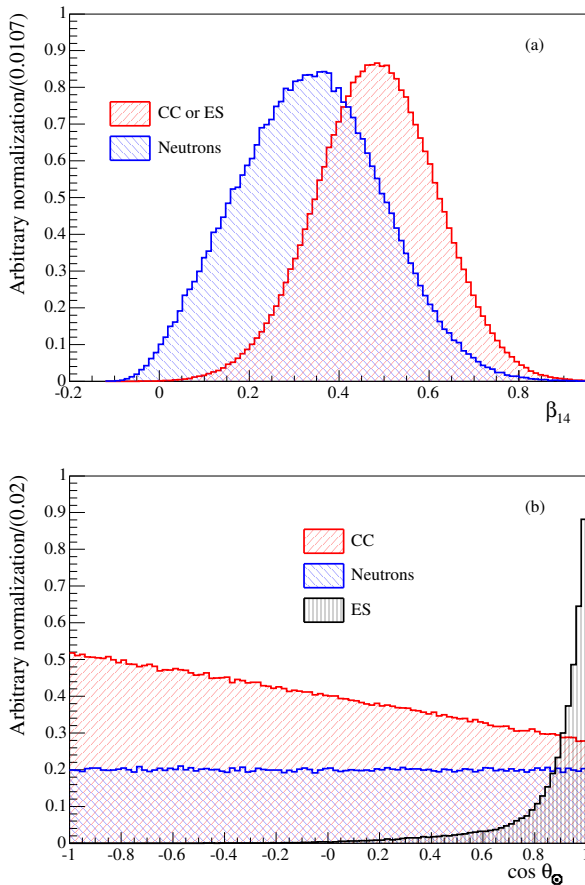


Fig. 5. β_{14} (a), and $\cos \theta_{\odot}$ (b) distribution for NC, CC, ES, and external neutron events. Where internal and external distributions are identical the distribution is simply labeled neutrons. Note that the distribution normalizations are arbitrary and chosen to allow the shape differences to be seen clearly.

number of triggered PMTs, the PMT trigger times and positions of an event. The variables are the effective electron kinetic energy, T_{eff} , a parameterisation of event isotropy, β_{14} , a parameterisation of the reconstructed radial position of the event ρ , and the cosine of the reconstructed event direction with respect to the Sun, $\cos \theta_{\odot}$.

The event position is parameterised by the volume-weighted radial position:

$$\rho = \left(\frac{R}{R_{\text{AV}}} \right)^3, \quad (1)$$

where R is the radius of the reconstructed event position and R_{AV} is the radius of the acrylic vessel (600.5 cm). The event isotropy is determined by the spatial distribution of triggered PMTs in an event and is parameterised as

$$\beta_{14} = \beta_1 + 4\beta_4 \quad (2)$$

with

$$\beta_l = \frac{2}{N(N-1)} \sum_{i=1}^{N-1} \sum_{j=i+1}^N P_l(\cos \theta_{ij}), \quad (3)$$

where P_l is the Legendre polynomial of order l , N is the total number of trigger PMTs in the event, and $\cos \theta_{ij}$ is the angle between PMTs i and j relative to the reconstructed event vertex.

There is a small background of external neutrons (EN) created by radiation outside the D_2O volume that can be separated using these observables. Background neutrons produced inside the D_2O volume (for example, produced by photodisintegration of deuterium by γ 's from the low levels of natural radioactivity) are determined by separate analyses and extracted after the fit.

Detailed Monte Carlo simulations are used to generate probability density functions (PDFs) characterizing signal distributions and are shown in figs. 4 and 5. These PDFs are used in an extended maximum-likelihood fit to the 4722-event dataset to extract the electron neutrino energy spectrum, ^8B neutrino fluxes, and day-night asymmetries. As some neutrino oscillation scenarios can distort the electron neutrino spectrum, the energy distribution of the CC and ES interaction was not assumed. For these two signals PDFs were created separately for each 0.5 MeV interval in the range 5.5–13.5 MeV. For $T_{\text{eff}} > 13.5$ MeV a single bin was used due to the low statistics in this energy region. A single PDF was used, for both the NC and EN components whose T_{eff} spectra are determined by the energy release of neutron capture on ^{35}Cl are independent of neutrino energy. The normalisation for each of these PDFs was allowed to vary in the fit giving a model-independent measurement of the neutrino energy spectrum.

To take the correlations between the four variables, multi-dimensional PDFs were used. Ideally a 4-dimensional PDF should be used, which would take into account all correlations automatically. Unfortunately, statistical limitations made this unpractical. The two following factorisations were considered:

$$P(T_{\text{eff}}, \beta_{14}, \rho, \cos \theta_{\odot}) = P(T_{\text{eff}}, \beta_{14}) \times P(\cos \theta_{\odot}) \times P(\rho) \quad (4)$$

and

$$P(T_{\text{eff}}, \beta_{14}, \rho, \cos \theta_{\odot}) = P(T_{\text{eff}}, \beta_{14}, \rho) \times P(\cos \theta_{\odot} | T_{\text{eff}}, \rho). \quad (5)$$

Both factorisations were tested by applying the signal extraction procedure to 100 Monte Carlo datasets. It was found that the parameterisation in eq. (4) resulted in a small bias. Equation (5) showed no sign of bias. This reduction in bias can be understood by the inclusion of correlations with ρ and $\cos \theta_{\odot}$ in eq. (5). When the expected bias was corrected for, both approaches gave consistent results when applied to the data.

3.2 Systematic uncertainties

Systematic uncertainties in detector response are evaluated through comparisons of Monte Carlo simulations and calibration data. The primary calibration sources used to study systematic uncertainties are a ^{16}N 6.13 MeV γ -ray

source and a ^{252}Cf fission neutron source. The ^{16}N source is used to study energy response, event reconstruction performance, and detector stability over time. The ^{252}Cf source is used to evaluate neutron response characteristics. Systematic uncertainties are propagated by perturbing the PDFs according to the estimated 1σ variation in each response parameter, and then repeating the signal extraction process. The dominant systematic uncertainties on the CC and NC extracted fluxes in the energy-unconstrained analysis are due to uncertainties in the β_{14} parameters. Uncertainties of less than a percent in the mean isotropy values translate to uncertainties of around 4% in the CC and NC fluxes. The energy scale uncertainty in the salt phase is estimated to be 1.15%, which contributes a 3.5% uncertainty in the NC flux, but has a smaller effect on the CC and ES fluxes. A radial scaling uncertainty of 1% is also one of the larger contributions to the overall systematic error, contributing roughly a 3% uncertainty to each flux. The ES flux uncertainty is dominated by a 5% systematic uncertainty due to the uncertainty in angular resolution. These are the major contributions to the systematic errors for the unconstrained analysis.

4 Results

4.1 Solar neutrino flux results

The energy unconstrained analysis as described in sect. 3.1 classified 2010 ± 85 events as NC, 2176 ± 78 as CC, and 279 ± 26 events as ES. The external neutron background is found to be 128 ± 28 events. Accounting for acceptance factors and detector lifetime, we can convert these extracted event numbers into equivalent ^8B solar neutrino fluxes:

$$\begin{aligned}\phi_{\text{NC}} &= 4.94_{-0.21}^{+0.21}(\text{stat})_{-0.34}^{+0.38}(\text{syst}), \\ \phi_{\text{CC}} &= 1.68_{-0.06}^{+0.06}(\text{stat})_{-0.09}^{+0.08}(\text{syst}), \\ \phi_{\text{ES}} &= 2.35_{-0.22}^{+0.22}(\text{stat})_{-0.15}^{+0.15}(\text{syst}),\end{aligned}\quad (6)$$

in units of $10^6 \text{ cm}^{-2} \text{ s}^{-1}$.

The flavour composition of the detected ^8B by SNO is illustrated in fig. 6.

4.2 Charged-current spectrum

Figure 7 shows the extracted recoil electron energy spectrum from the CC reaction obtained from the extended maximum-likelihood fit. Statistical uncertainties are shown around the data points, whilst the systematic uncertainties are shown with respect to the prediction for an undistorted ^8B shape. While some uncertainties may change the PDF shapes leading to a change in the fitted number of events, other simply affect the overall acceptance of events. Both must be accounted for as the latter can lead to errors in the translation of differential event counts into differential neutrino fluxes.

The measured spectrum is consistent with no distortions, and also with the best-fit MSW model, corresponding to the Large Mixing Angle (LMA) region of the solar

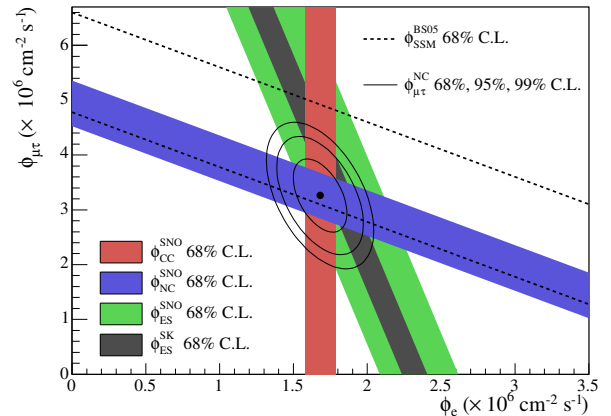


Fig. 6. Flux of μ and τ neutrinos *versus* flux of electron neutrinos. CC, NC, and ES flux measurements are indicated by the filled bands. The total ^8B solar neutrino predicted by the Standard Solar Model [2] is shown as dashed lines, and that measured with the NC channel is shown as the solid band parallel to the model predictions. The narrow band parallel to the SNO ES results corresponds to the Super-Kamiokande results in [7]. The intercepts of these with the axis represent the $\pm 1\sigma$ uncertainties. The non-zero value of $\phi_{\mu\tau}$ provides strong evidence for neutrino flavour transformation. The point represents ϕ_e for the CC flux and $\phi_{\mu\tau}$ from the NC-CC difference with 68%, 95% and 99% C.L. contours included.

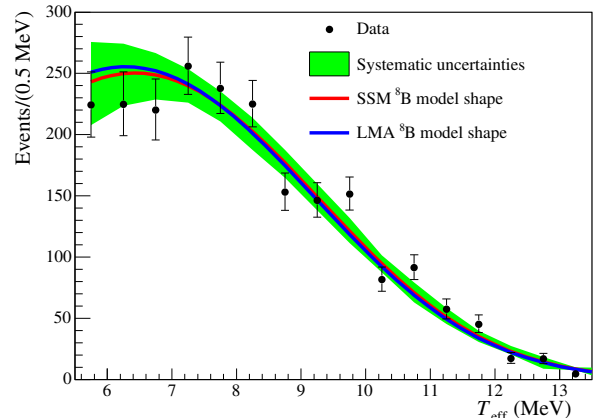


Fig. 7. The extracted CC T_{eff} spectrum with statistical error bars compared to the predictions for both an undistorted ^8B shape and the shape expected for the best-fit MSW model, corresponding to the LMA region, with combined systematic uncertainties, including both shape and acceptance components.

neutrino parameter space. The LMA spectrum does not differ significantly from the undistorted ^8B shape.

4.3 Day-night asymmetry measurement

For certain regions of mixing parameters, the MSW effect predicts a regeneration of solar electron neutrinos when the solar neutrino flux passes through the Earth.

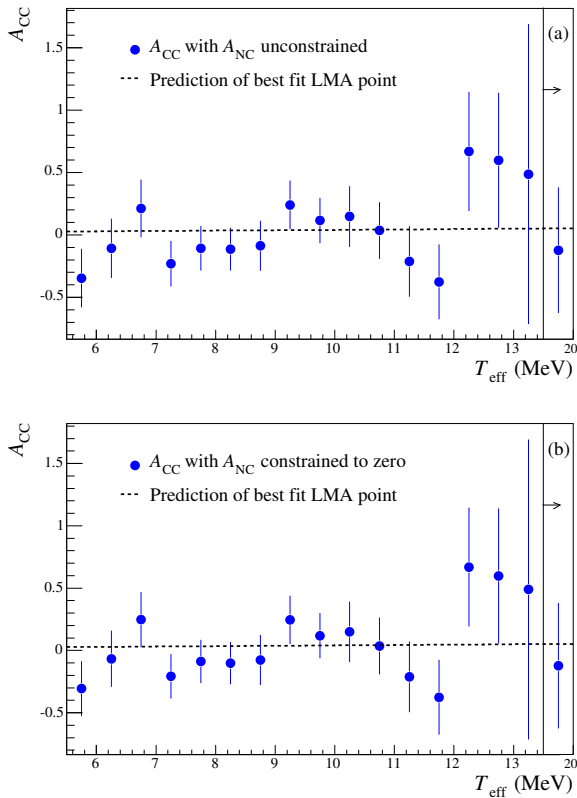


Fig. 8. Day-night asymmetries on each CC energy bin as a function of electron energy. Panel (a) shows the case in which no constraint is made on A_{NC} . Panel (b) shows the case in which A_{NC} is constrained to zero. The vertical lines show the expectation for $\Delta m^2 = 7 \times 10^{-5} \text{ eV}^2$ and $\tan^2 \theta = 0.40$.

The regeneration is measurable as an asymmetry of the solar flux:

$$A_{\text{DN}} = 2 \frac{\phi_{\text{N}} - \phi_{\text{D}}}{\phi_{\text{N}} + \phi_{\text{D}}}, \quad (7)$$

where ϕ_{N} is the solar flux measured during the night and ϕ_{D} is the solar flux measured during the day. The energy-unconstrained analysis carried out as described in sect. 3.1 was carried out separately for the day and night neutrino candidate events. The resulting asymmetries in the fluxes are

$$\begin{aligned} A_{\text{NC}} &= +0.042 \pm 0.086(\text{stat}) \pm 0.072(\text{syst}), \\ A_{\text{CC}} &= -0.050 \pm 0.074(\text{stat}) \pm 0.053(\text{syst}), \\ A_{\text{ES}} &= +0.146 \pm 0.198(\text{stat}) \pm 0.033(\text{syst}). \end{aligned} \quad (8)$$

An asymmetry in the NC flux could indicate that the solar flux contains sterile neutrinos or that unexpected interactions inside the Earth take place. Figure 8 shows the day-night asymmetry of the CC flux, sensitive to the electron neutrino component of the solar flux only, as a function of energy for the assumption the A_{NC} equals zero or can be different from zero.

Within the uncertainties the asymmetries are compatible with both zero and with the LMA solution.

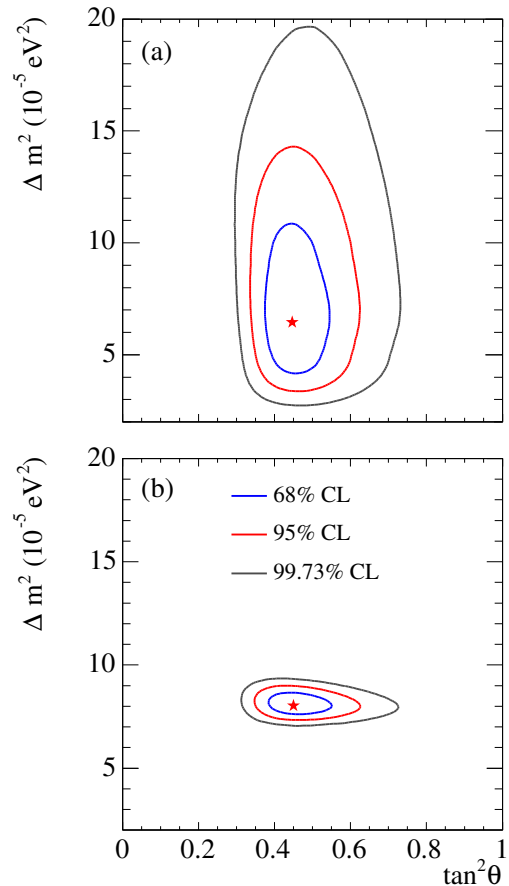


Fig. 9. Panel (a) shows the global neutrino analysis using only solar neutrino data, and panel (b) includes KamLAND's 766 ton-year data. The solar neutrino data included SNO's pure D_2O phase day and night spectra, SNO's salt phase extracted day and night CC spectra and ES and NC fluxes, the rate measurements from Cl, SAGE, Gallex/GNO, and SK-I zenith spectra. The ${}^8\text{B}$ flux was free in the fit, hep solar neutrinos were fixed at $9.3 \times 10^3 \text{ cm}^{-2} \text{ s}^{-1}$. The stars are plotted at the best-fit parameters from the χ^2 analysis.

4.4 MSW parameter constraints

The salt phase results for the fluxes, spectra, and day-night asymmetries can be combined with SNO's previous results and the results of other solar neutrino experiments to produce constraints on the fundamental neutrino parameters in the MSW model. Figure 9(a) shows the results of a global χ^2 analysis. The best-fit point is $\Delta m^2 = (6.5_{-2.3}^{+0.4}) \times 10^{-5} \text{ eV}^2$ and $\tan^2 \theta = 0.45_{-0.08}^{+0.09}$.

Including the results for the KamLAND experiment [8, 9], the best-fit point is found to be

$$\begin{aligned} \Delta m^2 &= (8.0_{-0.4}^{+0.6}) \times 10^{-5} \text{ eV}^2, \\ \tan^2 \theta &= 0.45_{-0.07}^{+0.09}. \end{aligned} \quad (9)$$

The ‘‘survival probability’’ for solar neutrinos, which can be determined by SNO from the measurement of the ratio of the CC and the NC flux, places strong constraints

on the value of $\tan^2 \theta$. Measurements of the NC rate in the third phase of the SNO experiment will further improve determinations of the fundamental neutrino oscillation parameters.

5 Conclusions

New results from the salt phase of the SNO experiment have been summarised, including a measurement of the flux of ^8B solar electron neutrinos through the CC reaction and a measurement of the ^8B solar neutrinos of all flavours through the neutral-current reaction. The use of the isotropy parameter as a tool to statistically separate the CC and NC events allows a model-independent measurement of the solar neutrino fluxes in the salt phase. The flux results confirm and improve previous results, demonstrating solar neutrino flavour change and contributing to evidence for solar neutrino oscillations.

Global analysis of solar neutrino and KamLAND data strongly favour LMA oscillations. The oscillation parameter space has now been tightly constrained to a region where the predicted distortion to the ^8B energy spectrum is small. The measured energy spectrum derived from the CC reaction is consistent with the expected spectrum assuming an undistorted ^8B shape, as well as with the predicted spectrum consistent with the best-fit LMA parameters. The day-night flux asymmetries predicted for the LMA scenario are also small and the day-night asymmetries measured here are consistent with these predictions, as well as with no day-night effect.

6 Outlook

Improved precision in the NC flux measurement is expected from the third phase of SNO. The salt was removed from the detector in October 2003, in preparation of the

installation of the neutral-current detectors (NCDs). Forty string of ^3He proportional counters with a total length of approximately 350 m have been installed into the D_2O volume. This will provide an independent measurement of the NC flux on an event-by-event basis. The neutron capture mechanism of the counters is:



The counters have been successfully installed into SNO and production data taking started at the beginning of 2005.

This research was supported by Canada: Natural Sciences and Engineering Research Council, Industry Canada, National Research Council, Northern Ontario Heritage Fund, Atomic Energy of Canada, Ltd., Ontario Power Generation, High Performance Computing Virtual Laboratory, Canada Foundation for Innovation; US: Department of Energy, National Energy Research Scientific Computing Center; UK: Particle and Physics and Astronomy Research Council.

References

1. Bruce T. Cleveland *et al.*, *Astrophys. J.* **496**, 505 (1998).
2. J.N. Bahcall, A.M. Serenelli, S. Basu, arXiv:astro-ph/0412440.
3. The SNO Collaboration, *Phys. Rev. Lett.* **87**, 011301 (2002).
4. The SNO Collaboration, *Phys. Rev. Lett.* **89**, 181301 (2004).
5. The SNO Collaboration, *Phys. Rev. C* **72**, 055502 (2005), arXiv:nucl-ex/0502021.
6. The SNO Collaboration, *Nucl. Instrum. Methods A* **449**, 172 (2005).
7. S. Fukuda *et al.*, *Phys. Lett. B* **539**, 179 (2002).
8. K. Eguchi *et al.*, *Phys. Rev. Lett.* **90**, 021802 (2003).
9. T. Araki *et al.*, arXiv:hep-ex/0406035.